J Mater Sci: Mater Med (2010) 21:2989–2998
DOI 10.1007/s10856-010-4149-7

Scaffold percolative efficiency: in vitro evaluation of the structural criterion for electrospun mats

Ashkan Heidarkhan Tehrani · Ali Zadhoush · Saeed Karbasi · Hojjat Sadeghi-Aliabadi

Received: 23 May 2010 / Accepted: 6 August 2010 / Published online: 29 August 2010

Abstract Fibrous scaffolds of engineered structures can be chosen as promising porous environments when an approved criterion validates their applicability for a specific medical purpose. For such biomaterials, this paper sought to investigate various structural characteristics in order to determine whether they are appropriate descriptors. A number of poly(3-hydroxybutyrate) scaffolds were electrospun; each of which possessed a distinguished architecture when their material and processing conditions were altered. Subsequent culture of mouse fibroblast cells (L929) was carried out to evaluate the cells viability on each scaffold after their attachment for 24 h and proliferation for 48 and 72 h. The scaffolds' porosity, pores number, pores size and distribution were quantified and none could establish a relationship with the viability results. Virtual reconstruction of the mats introduced an authentic criterion, "Scaffold Percolative Efficiency" (SPE), with which the above descriptors were addressed collectively. It was hypothesized to be able to quantify the efficacy of fibrous scaffolds by considering the integration of porosity and interconnectivity of the pores. There was a correlation of 80% as a good agreement between the SPE values and the spectrophotometer absorbance of viable cells; a viability of more than 350% in comparison to that of the controls.

A. Heidarkhan Tehrani · A. Zadhoush (✉)
Department of Textile Engineering, Isfahan University of Technology, 84156-83111 Isfahan, Iran
e-mail: zadhoush@cc.iut.ac.ir

S. Karbasi
Medical Physics and Biomedical Engineering Group, Department of Medicine, Isfahan University of Medical Sciences, 81746-73461 Isfahan, Iran

H. Sadeghi-Aliabadi
Department of Pharmaceutical Chemistry, School of Pharmacy, Isfahan University of Medical Sciences, 81746-73461 Isfahan, Iran

1 Introduction

Organ retrieval is the most prime task to be accomplished when tissue malfunction occurs and previously a practical form of reconstruction was expected to be the implantation. It was within this context that the field of tissue engineering emerged and porous scaffolds were built to help the new tissue to develop and regenerate. In course of the challenge to imitate nature, physicians try to optimize the environment of the infected area by maximizing the nutrition and waste delivery and minimizing any hostile activity. For scaffolds, the same story takes place at a cellular level [1, 2].

Scaffolds incorporate viable cells to promote tissue regeneration. Their porous architecture determines the quality of mass diffusion and transportation phenomena which finally determines its permeability. A 3D conduit for cells growth, scaffolds evolves infiltration and phenotypic regulation of a desired cell type [3]. In addition to these essentials, a suitable construct possesses such structural properties that are optimized for attachment and migration of cells. They may include provision of adequate mechanical strength, maximizing surface area for attachment and growth, the inclusion of large pore volumes to accommodate and deliver a cell mass sufficient for tissue repair, strong pore interconnectivity for transport of nutrients and waste products to and from the implant [4]. Accordingly, controlling the architectural structure is truly a key factor in designing scaffolds; however, there has been no accurate criterion for designing an optimal structure yet [5].

Electrospinning is a simple process used for fabricating fibrous mats which can structurally mimic the extracellular matrix (ECM) [6]. The architectural characteristic of the resulted mat can be deliberately altered when various material and processing parameters are manipulated [7]. The only challenging aspect of electrospinning is the difficulty of controlling scaffolds pores and consequently the architecture of the interconnection and the resulting permeability [8]. This is due to the fact that the cylindrical pores of other processing techniques have not been produced herein [9]. In fact, these mats are merely a group of nonwoven fibers lying loosely upon one another. Aside from the inherent dynamic rendering of the apertures in electrospun mats, it is imperative to report the architectural properties to determine the characteristic of successful electrospun ECM analogues [10].

Structural properties of the scaffolds have been characterized with different techniques based on their architectures. Mercury intrusion porosimetry provides information concerning porosity; however, it cannot detect isolated pores within the scaffolds, neither does it discriminate connections between the pores based on their diameters [11]. Being limited due to the severe dependence on the required fluid flow pressure, this method is more troublesome when it applies to materials that have irregular pore geometries as in electrospun fibrous scaffolds. X-ray micro-computed tomography (μCT) has been previously used in medical applications [12]. Despite being nondestructive in recent advances, μCT has not been fully exploited for the description of voids space interconnectivity. Scanning electron microscopy with the capability of showing high detailed topologies represents the pores interconnectivity extremely qualitative [9]. In general, the information obtained from these techniques is insufficient for a precise assessment of the pore interconnectivity to correlate with or predict the biological performance [13]. All these techniques count on no reliable evidence for answering the question whether a scaffold is applicable. There has been no clear consensus regarding which methods and variables are relevant to evaluate the cell adhesion affinity within the scaffolds quantitatively [14].

In this work, we investigated the correlation between well known architectural characteristics of fibrous scaffolds and the viability results obtained from their in vitro assessment. We demonstrate the application of digital image analysis to reconstruct the 3D skeletal configuration of fibrous scaffolds, probing into their spatial structure in order to quantify porosity, pore size, pore numbers and their distribution accurately. A criterion based on both the porosity and the connectivity of the inner aperture was derived as "Scaffold Percolative Efficiency" (SPE); hypothesized to be capable of substantiating fibrous scaffold applicability. Various scaffolds of poly(3-hydroxybutyrate) (P3HB) were electrospun with different architectural characteristics and seeded with mouse fibroblast (L929) cells. The cells viability accounts for the structural efficiency of the corresponding scaffolds and so did the SPE values. They were supposed to show the quality of how cells can attach and proliferate. The correlation between the SPE's values and the spectrophotometer absorbance of viable cells was determined to examine whether this criterion can reliably indicate an applicable scaffold for a specific biomedical purpose.

2 Materials and methods

Poly(3-Hydroxybutyrate) (P3HB; Mw = 300,000 g mol^{-1}) natural origin powder were purchased from Sigma-Aldrich, USA, and used as received without further purification. Chloroform and Dimethylformamide (DMF) were bought from Merck, Germany. A flask of growing mouse fibroblast cells (L929) was purchased from Pasteur Institute of Iran (IPI) and maintained in incubator at 37°C in a humidified atmosphere containing 5% CO_2. RPMI 1640 medium and Trypsin were both bought from Sigma-Aldrich, USA, and Phosphate buffer saline (PBS) was purchased from Gibco, Scotland.

2.1 Experimental design

Upon fabricating electrospun mats, different adjustments of solution and processing parameters can alter fibers diameter and their orientation. Manipulating these parameters results in production of scaffolds with diverse architectural characteristic [15–19]. Tehrani et al. have previously studied the most governing parameters in electrospinning fibrous P3HB scaffolds through a L16 Taguchi orthogonal matrix [20]. Each of the produced scaffolds possessed different morphology and porous structure when polymer content, solvent and co-solvent mixture, nozzle-collector distance and applied voltage were altered. Aside from the logic behind choosing the number of levels, their limits were confined in a way that the entire trials were processable (Table 1). The conditions and the levels of the parameters followed the design shown in Table 2.

2.2 Electrospinning setup

A syringe pump was used to force a solution of 1 cm^3 through a small-diameter capillary (ID = 0.5 mm); forming a pendant drop at the tip. A positive electrode from a high adjustable regulated power supply was then directly attached to the metal needle. A homemade collector was built to ease the deposition of dense square mats for further image analyses. The collector's face was covered and

Table 1 Each level was assigned to a specified condition for both processing and material parameters

Control factor	Level				Unit
	1	2	3	4	
Polymer content	6	8	10	12	%wt
Applied voltage	8	10	12	14	kV
Nozzle distance	15	25	_	_	cm
Solution mixture	100:0	90:10	_	_	_

Table 2 Taguchi L16 orthogonal matrix, was used for fabricating the scaffolds. Material and processing parameters were adjusted according to the digits specified in Table 1

Run No.	Polymer Content	Applied Voltage	Nozzle Distance	Solution Mixture
1	1	1	1	1
2	1	2	1	1
3	1	3	2	2
4	1	4	2	2
5	2	1	1	2
6	2	2	1	2
7	2	3	2	1
8	2	4	2	1
9	3	1	2	1
10	3	2	2	1
11	3	3	1	2
12	3	4	1	2
13	4	1	2	2
14	4	2	2	2
15	4	3	1	1
16	4	4	1	1

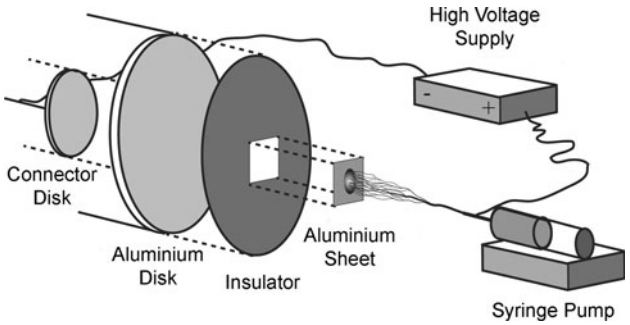

Fig. 1 A circular aluminum sheet of 20 cm radius was used as a collector, not only to distribute the charge density uniformly but to enable the fibrous layers accumulated in its center

insulated with a rubber film, except a square of 1 × 1 cm^2 where an aluminum sheet of the same size was placed for the scaffolds to be collected without difficulty (Fig. 1).

2.3 Fibrous structural reconstruction

Having sixteen scaffolds acquired from the trials, they were mounted on a 4 × 4 cm^2 aluminum sheet and coated with gold in a (BALTEC SCD 005) sputtering device at 5 mA for 3 min. The images were captured with (PHILIPS XLS 30 Series; Netherland) scanning electron microscope from 6 different arbitrary spots for each scaffold. All the images had the same magnification of 750 times and were captured with the same brightness and contrast. Writing a program code in MATLAB (R2007a), porosity was represented as the ratio between the empty spaces to the whole volume the scaffold occupies. This is mathematically presented in Eq. 1 [21]

$$P = (V_o/V_T) \tag{1}$$

where P is the porosity of the scaffold, V_o is the magnitude of open voids and V_T considered as the total volume of the scaffold. Although, usage of the term porosity with the above ratio is common for thick three dimensional structures, for thin nonwoven fabric as nanofibrous mats the same expression can be defined by Eq. 2 [22]

$$P = (A_o/A_T) = \left(\sum_{i=1}^{n} a_i \Big/ A_T\right) \tag{2}$$

where A_o is the area of open apertures in a 2D layer, A_T is the total area, a_i is the area of pore i and n is the total number of pores. The layers thickness can be approximated by the fibers diameter in electrospinning. For a 3D scaffold, porosity can be calculated with the above ratio only if a layer, which is as thick as its fibers, can be extracted. This was done when the threshold shown in Eq. 3 was used whilst the SEM grayscale images were converted to binary mode [23]

$$h = ((\mu + \sigma)/256) \tag{3}$$

Here h is the threshold, μ is the mean intensity of the image pixels and σ is the standard deviation. The maximum intensity in the grayscale images was 256.

All the images were cropped in the same size of 420 × 720. Successive morphological operations enabled the removal of either the residual fibers in layers beneath or any unwanted noise. Pores were assumed as objects and labeled accordingly. Open areas were counted and their equivalent radius was computed. The mean porosity was computed by averaging between $m = 6$ arbitrary images using Eq. 4

$$\bar{P} = \frac{1}{m}\sum_{i=1}^{m} P_i = \frac{1}{m}\sum_{i=1}^{m}\sum_{j=1}^{n}\frac{a_{ij}}{A} = \frac{1}{mA}\sum_{i=1}^{m}\sum_{j=1}^{n} a_{ij} \tag{4}$$

where n is the number of the open areas found on the surface, A is the total scanned area, a_{ij} is the area of the

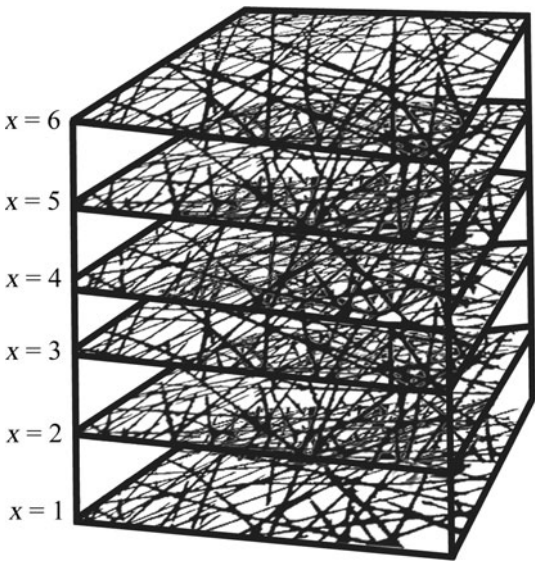

Fig. 2 3-Dimensional reconstructed fibrous scaffold with $x = 6$ deposited random layers all of which obtained from a single specimen with polymer concentration of 8 wt%, 12 kV of applied voltage and neat chloroform at the nozzle distance of 25 cm from the collector

pore j found on the image i of the corresponding scaffold. P_i is the porosity calculated based on the image number (i).

Repetition of the six layers on one another simulated the actual structure of an electrospun scaffold. By adding a new layer, some open areas of the previous ones may be overlapped. As a result, a gradual reduction in the remaining open areas as a function of the deposited layers was derived. Considering x as the number of layers we have,

$$R_x = \left(\sum_{i=0}^{n} a_i \Big/ A_{\mathrm{T}} \right)_x \tag{5}$$

where R_x is a discrete function which shows the remaining open areas after having x layers deposited (Fig. 2). In order to estimate the number of layers required for R_x to become zero, an exponential curve was fitted on these points. The relationship between the number of deposited layers x and their consequent remaining open areas $F(x)$ is presented by Eq. 6.

$$F(x) = a \times e^{bx} \quad -1 < b < 0,\ a > 0 \tag{6}$$

where the coefficient a and the exponent b are constants.

2.4 Cell culture and cell seeding

Mouse connective tissue fibroblast-like cells (L929) were cultured in RPMI 1640 medium. The medium was replaced every 2 days; in the meantime, the cells were counted with hemacytometer to see if they reached to a required number for having 4×10^4 of them per well. In the course of incubation the culture mediums were maintained at 37°C in a humidified atmosphere containing 5% CO_2. After the cells grown to confluence, they were digested by 1 ml 0.25% trypsin for 1–2 min. Subsequently, 3 ml of culture medium was added to stop digestion prior to centrifuging the solution which resulted in the separation of the detached cells.

Each of the 16 scaffolds was punched into circular discs of about 7 mm in diameter with a borer and placed in a sterile 96-well tissue-culture polystyrene plate (TCPS). The wells diameter was 5 mm at the bottom, so the scaffolds extended perimeter made a hold onto its wall and restrained at the very end. Despite the lower density of the thin specimens than the culture medium and their porous structure in which air may reserve, none of them let float. As the resistance of the P3HB scaffolds to UV and alcohol was fair enough for a convectional sterilization process, they were submerged in 70% ethanol for 1 h and exposed to Ultra Violet (UV) light for another hour. They were washed with autoclaved deionized water and conditioned with a serum free RPMI 1640 culture medium for 12 h to ensure a complete contact between the specimens and the wells. The dispersion of incubated L929 cells in RPMI 1640 culture medium supplemented with 10% fetal bovine serum was finally seeded on each and every one of the specimens and the empty wells of TCPS as well.

2.5 Cell attachment and proliferation (MTT assay)

L929 cells were first allowed to attach to the specimens and TCPS for 24 h. Cells proliferation was determined after 48 and 72 h. Samples were rinsed with 200 µl/well phosphate buffer saline I order that the unattached cells were removed prior to MTT assay. Reduction of the yellow tetrazolium salt to purple formazan crystals by dehydrogenase enzymes which is secreted from the mitochondria of metabolically active cells is the mechanism of MTT assay. The amount of purple formazan crystals formed was proportional to the number of viable cells. Hence a mixture of 70:30 serum free culture medium and MTT solution was added to each well. The whole plates were incubated at 37°C for 3 h. MTT solution and the culture medium were removed and the remaining formazan crystals were dissolved with 150 µl/well dimethylsulfoxide (DMSO). Pipetting the solution for 15 min, the TCPS plates were then transferred into a micro-plate reader (Elisa spectrophotometer), in which the absorbance at the wavelength of 540 nm represented the number of viable cells.

2.6 Morphological observation

From each cultured period, one set of scaffolds, which were produced in similar processing and material conditions,

were chosen for morphological observation. The specimens were rinsed with PBS and fixed with 3% glutaraldehyde solution. After 30 min, they were rinsed again with PBS and kept for an hour. Specimens were dehydrated in ethanol solutions of varying concentration (30, 50, 70, 90, and 100%, respectively) and soaked for 10 min at each concentration and let dry in air. Finally, they were mounted on an aluminum sheet and coated with gold in a (BALTEC SCD 005) sputtering device at 5 mA for 3 min. The SEM images were captured with (PHILIPS XLS 30 Series; Netherland) scanning electron microscope.

2.7 Statistical analysis

The statistical analysis of the structural data, regressions, scatter-plots and the correlation between the SPE values, which were derived from the simulation, and viability results, which were obtained from the in vitro cell culture, were all calculated with the help of SPSS 13.0 software (SPSS Inc. IBM Company, Chicago, Illinois, USA). Through all these, P values smaller than 0.05 were considered statistically significant.

3 Result

Having designed appropriate condition of levels, all the trails were carried out successfully; fabricating electrospun mats of smooth P3HB fibers. Through Taguchi orthogonal arrays, scaffolds with distinguished structural architecture were produced. A selection of the resulted mats is presented in Fig. 3.

According to different conditions with which the scaffolds were prepared, each one possessed distinguished pore size, pore geometry, size and distribution. The channels, which were formed as the result of the layers deposition, varied in diameter and their path deviated through the three dimensional structure. All the fabricated mats had fibers diameter of about 500 nm to 2 μm; these boundaries were determined to be for run number 4 and 15 respectively (Table 1). The mean porosity of the scaffolds was confined in a range between 65% for run number 1 and 85% for 8.

3.1 Web permeability index

In the reconstructed model, dead end channels development varied due to the architectural characteristic of the pores. The more the pores were interconnected, the further the channels penetrated and as a result greater numbers of layers were required for the scaffold's apertures to be blocked. Observing the formation of the 3-dimensional structure through an axis perpendicular to the layers surface, the reduction of the open areas in accordance to the number of deposited layers became clear (Fig. 4).

Mathematically, infinite number of layers was required for $F(x)$ to reach zero (Eq. 6). Instead of approximating the root and finding the equivalent numbers of layers, the nth derivations of the function $F(x)$ as in Eq. 6 was considered using Eq. 7.

$$F^{(n)}(x) = ab^{(n)}e^{bx} \tag{7}$$

Exponent b considered to be the prominent factor responsible for determining the rate with which the interconnected inner apertures blocked. The greater the value of b became the faster the dead end channel appeared. In another words, b can be considered as a measure of pores interconnectivity within a fibrous scaffold.

3.2 In vitro evaluation

The cultured cells in the control wells were still rounded in 5 h, while the cells on the scaffolds surface started to flatten; supposing that the cells prefer the latter. After 12 h

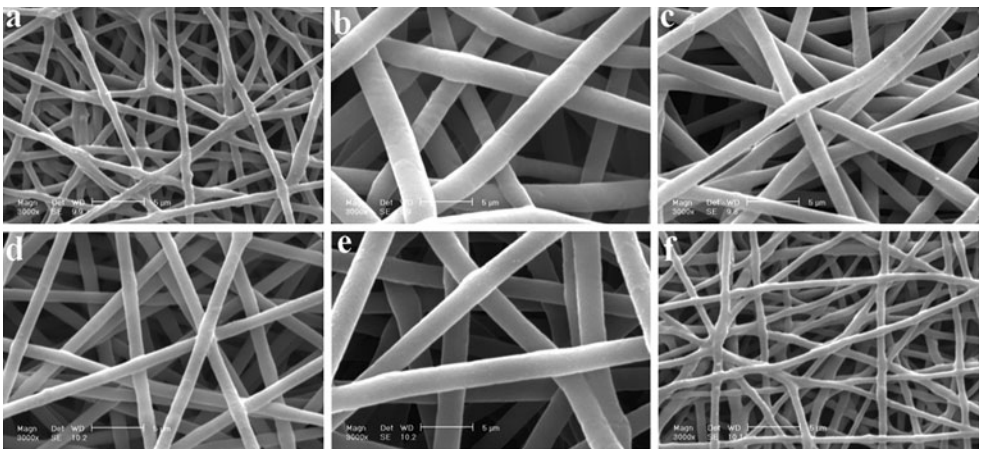

Fig. 3 Smooth P3HB fibrous scaffold without the presence of beads was obtained with the following polymer concentration, applied voltage, CF:DMF mixture and distance respectively; **a** 6 wt%, 12 kv, 25 cm, 90:10; **b** 8 wt%, 12 kv, 15 cm, 90:10; **c** 10 wt%, 14 kV, 25 cm, 100/0; **d** 8 wt%, 8 kV, 25 cm, 100/0; **e** 10 wt%, 14 kV, 15 cm, 100:90; **f** 6 wt%, 12 kV, 25 cm, 100:90

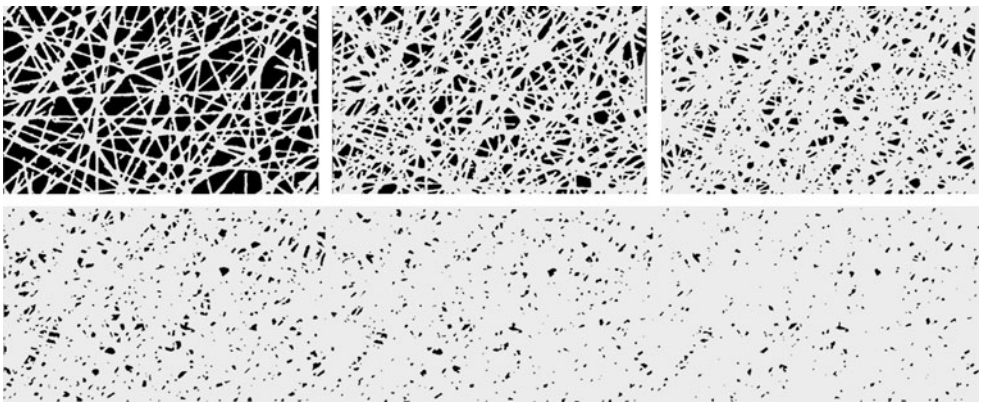

Fig. 4 The gradual reduction of remaining open areas after new layers overlap the beneath layer showing how fast the accessible spaces vanished (1–6)

of incubation, the attached cells on the fibrous scaffolds expanded completely and within 72 h the proliferated cells covered almost 30% of the P3HB scaffold. The viability of the cells cultured on TCPS was used as a reference in arriving at the conclusion that the mean viability was increased at least three times for the fibrous scaffolds; an increase up to 350% in comparison to that of the controls (Fig. 5).

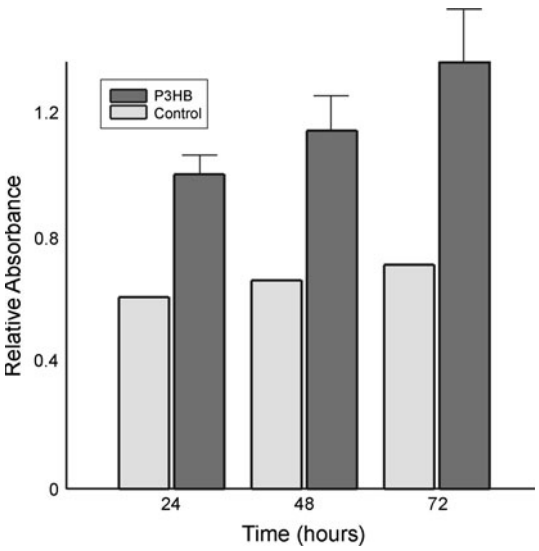

Fig. 5 The average cell viability of the fibrous scaffold for different culture time and their corresponding viable cells in controls

The gradual immigration of the cells into the porous structure depth can be illustrated when the increasing number of adhered cells on the P3HB walls was observed during their proliferation. Figure 6 shows SEM images of mouse fibroblast cells that were seeded on the surfaces of the fibrous scaffolds from 24 to 72 h.

3.3 Scaffold percolative efficiency

The porosity and the coarse architectural characteristic of the fibrous porous scaffolds were found to be inadequate descriptors [3]; however, with having the porosity (P) from Eq. 4 and a coefficient for assessing the permeability and interconnectivity within a scaffold from Eq. 6, a criterion based on these parameters was deduced.

The criterion was proposed to be a dimensionless number with which the efficacy can be addressed and also comprises both the volume porosity and the connectivity of individual inner pores. On that account, scaffold percolative efficiency (SPE) was introduced with Eq. 8.

$$\mathrm{SPE} = \frac{\bar{P}}{b} \tag{8}$$

This ratio was determined to be able to describe the accessibility of the inner voids within a fibrous scaffold. In this vulgar fraction, the mean porosity, the numerator, is advantageous to the efficacy (SPE) and the permeability index, the denominator, is not. Although various structural

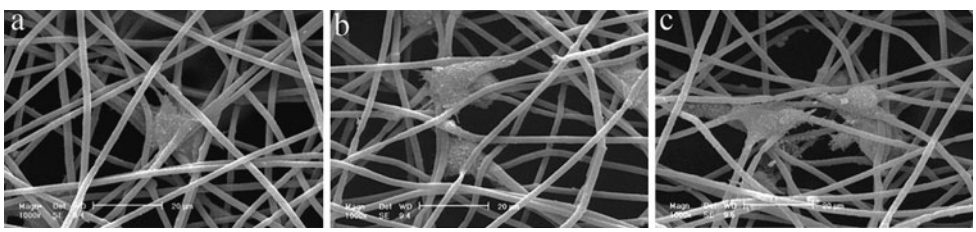

Fig. 6 The L929 cells infiltration depends on the pores architectural characteristics of a scaffold. **a** The attachment after 24 h; **b** The proliferation within 2 days; **c** and after 3 days of culture

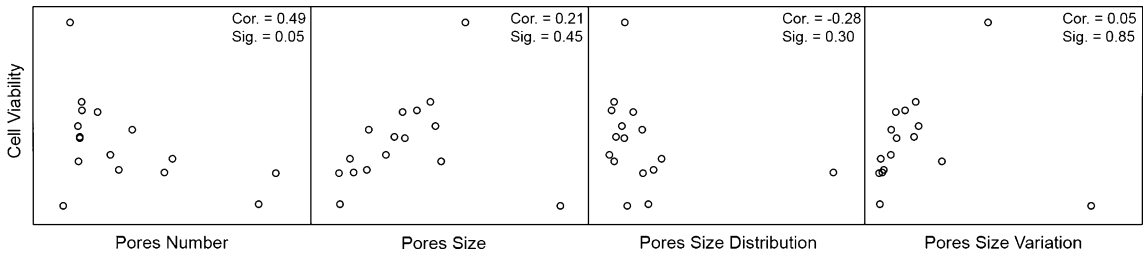

Fig. 7 The matrix scatter-plots of the in vitro results and their relative structural characteristics have shown no significant relationship between the variables. Each circle represents a scaffold out of the entire trials according to Table 2

characteristic as the mean pores size, their number, distribution and variation indicated no relationship with in vitro results (Fig. 7), the SPE values were in good agreement with the cell viability of their corresponding scaffolds. As the structural measurements were normally distributed, the association between the two variables was deduced with the Pearson correlation by removing the outliner data.

Figure 8 shows the resulting scatter-plot appears to be suitable for linear regression as a measure to evaluate the amplitude of the relationship between the simulation and the in vitro results. A correlation of 80% was calculated between the viability of the cultured cell after 72 h and the SPE values for the same scaffolds. The spectrophotometer relative absorbance of cultured medium were presented for the sake of comparison in Fig. 9. SPE values more than a hundred percent indicate that a scaffold with more interconnected channels can be more efficient and consequently preferred to a scaffold with high porosity but less interconnectivity.

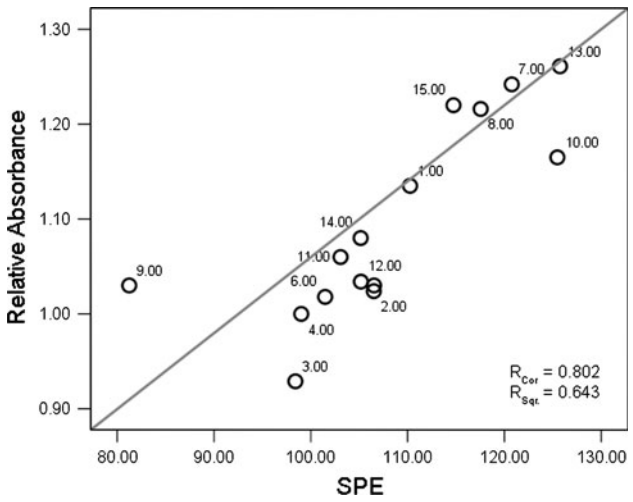

Fig. 8 R $_{Cor}$ is the multiple correlation coefficient; its large value (0.802) indicates a strong relationship between the variables. R_{Sqr} is the coefficient of determination; it shows that more than a half of the results were explained by the model

4 Discussion

It is impossible to understand the very complex interplay between the functionality of scaffolds from a structural point of view to a biological one; especially with purely empirical means that would require multiple time consuming experiments [24–27]. To reduce the number of experiments and to help the understanding of the obtained experimental results, theoretical models and simulations were developed [17, 18, 28, 29]. The L16 Taguchi orthogonal arrays stand for a fraction of the full-factorial combinations and were utilized here to build a matrix of experiment runs with the most contrasting conditions. In this work both the image analysis and the in vitro cell culture experiments have been carried out using two sets of specimens fabricated in accordance to the mentioned design.

From the structural analysis if a criterion could exist that reflects the scaffold efficiency based on a real biological evidence, it can definitely predict the suitability of such a structure quantitatively; aiming toward a specific tissue engineering purpose. This criterion has to be comprised of five important scaffold parameters: porosity, pore size and distribution, fenestration size and distribution, interconnectivity and pores orientation [30–33]. The integration of these parameters as a single criterion can use to assure an efficient permeability. This illustrates the necessity to quantify each individual pore and interconnect throughout the entire network; what was exactly fulfilled here with the image analysis and the modeling approach. The concept of two dimensional image processing was deliberately ignored when the actual 3-Dimensional structure of the fibrous scaffolds were reconstructed [34]. The modeling of such a structure was used to explore the interaction between biological applicability and the architectural characteristic of a scaffold.

Ideally, the neat forms of the renowned properties, like the porosity or their size were not able to predict the inherent efficacy of the descriptor itself [35]. It was evident that there was no meaningful correlation between these mere descriptors and in vitro assays. However, the fact still remains that the architectural characteristic of a scaffold

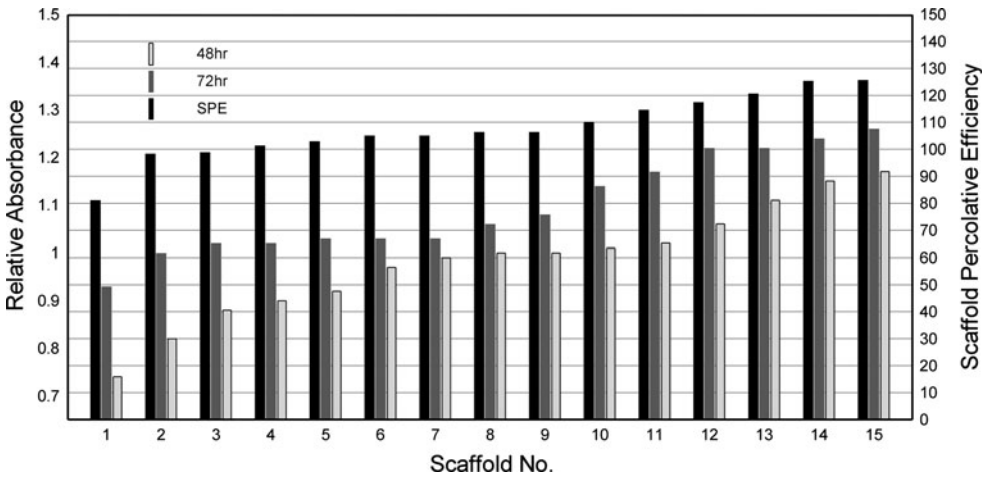

Fig. 9 The simulated SPE values and the experimental in vitro results shown a correlation coefficient of 0.75 and 0.45 with a significance level of 0.00 and 0.01 for 48 and 72 h of cell culture respectively

determines the transport phenomena within it [36–38]. The transportation comprises the nutrition and waste delivery and the quality of cell attachment and their following migration. All of these properties are governed by the scaffold porosity and permeability. For the later property, the exponent b in Eq. 7 seems to be an appropriate substitution while the role of the porosity still needs to be engaged with the concept.

The b indices stand for the pore interconnectivity, the accessible pore volume, or the overall permeability of a fibrous scaffold. Accessible pore volume can be defined as the total volume of pores which can be infiltrated from all peripheral borders to the interior of the scaffold [12, 32]. The accessible volume is the pore volume that is accessible from the outside of an object with a selected diameter. There was a reduction in voids space which remains accessible from outside as the layers of fibrous mats overlaps. To put light on the mechanism when the layers of electrospun fibers accumulate on one another, a projection view of the reducing inner aperture is illustrated in Fig. 10. The available infiltration space for an individual mass became less and less when succeeding layer deposited and eventually resulted in a blockage of the penetration sooner or later.

The size, geometry, orientation, interconnectivity and branching of pores and channels directly affect the nature of nutrient diffusion and tissue ingrowths [39, 40]. A pore can be defined as a void space within a scaffold, whereas porosity can be considered as a collection of pores. Some literatures report that high porosity can guarantees adequate space for cell-polymer interaction [41, 42]. What has often been ignored is that porosity measurement is not sufficient to evaluate scaffolds applicability but the pores in the scaffold need to be interconnected for efficient delivery as well. Generally, an increase in porosity leads to an increase in permeability, but for this to happen the pores need to be highly interconnected [35, 38]. Pore interconnectivity is a

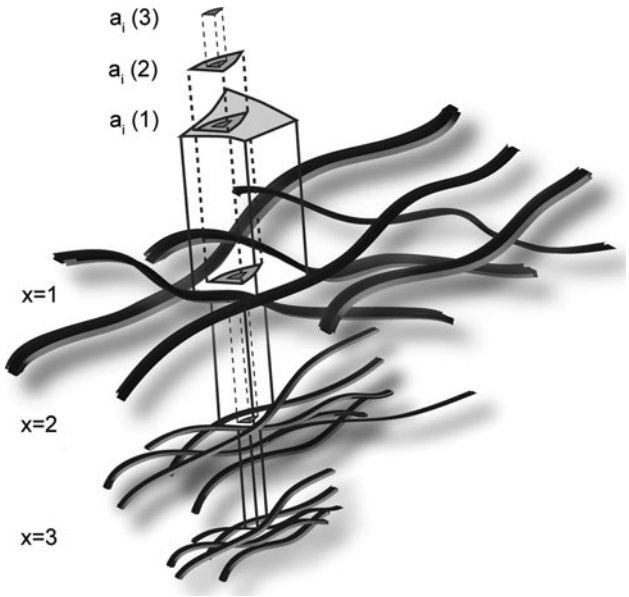

Fig. 10 The Projection of channel inlet for cells infiltration and the resulting reduction of areas (ai) when greater numbers of layers (x) accumulate

critical factor and is often overlooked in scaffold design and characterization. A scaffold may be porous, but unless the pores are highly interconnected, they serve no purpose and become superfluous in a scaffold for tissue engineering. The Scaffold Percolative Efficiency comprised the most dominant characteristic of a scaffold which was truly hypothesized as a prefigure to predict the actual biological response (Eq. 8).

According to Fig. 5 the number of viable cells increased when enough time was lent for their proliferation to dominate. The exponential growth of the cells viability on fibrous scaffolds within 3 days of culture can be compared with the negligible linear increase in the amount of the viable cells in control wells. For the controls, this can be due to the growth mere dependence on the culture time. On

the other hand the scaffolds porosity and high surface to volume ratio provided a substrate with lower energy level and higher biomaterial-cell interface. The augmented variation of the cells viability illustrated by the error bars in Fig. 5 was another evidence for the meaningful impact ($P < 0.05$) of the structural difference among the scaffolds. The more the scaffolds were structurally efficient, the more viable cell can be found as the days of culture went by and their difference became more vivid.

5 Conclusion

A review of the related literatures rarely showed a satisfactory quantitative definition of an ideal scaffold construct. The research presented in this work virtually reconstructed an electrospun fibrous mat not only to represent its actual 3D structure but also to let the characteristic evaluation perform at its most accurate possible level. The quantitative analysis provided the assessments of interconnectivity, porosity and consequently Scaffold Percolative Efficiency (SPE), a criterion that can address these properties all at once. The reliability of this criterion was validated with in vitro experiment, covering most biological aspect of the procedure. For various scaffolds that differed structurally, distinguished SPE values and viability results were obtained. It was determined that none of the raw characteristic of a scaffold can predict the actual behavior of the cultured cell; however, a comprehensive genuine parameter like SPE which represents a good correlation with in vitro results can be utilize to measure the efficiency for any electrospun fibrous scaffold. The differences among the scaffolds stood out when the duration of cultured cells were extended. The scaffold with higher porosity and of course more interconnected channels and as a result greater SPE values, possessed greater number of viable cells and determined more efficient.

References

1. Park JB, Bronzino JD. Biomaterials: principles and applications. 1st ed. New York: CRC Press; 2002.
2. Lanza RP, Langer R, Vacanti J. Principles of tissue engineering. 3rd ed. New York: Academic Press; 2007.
3. Laurencin CT, Nair LS. Nanotechnology and tissue engineering: the scaffold. 1st ed. New York: CRC Press; 2008.
4. Knackstedt MA, Arns CH, Senden TJ, Gross K. Structure and properties of clinical coralline implants measured via 3D imaging and analysis. Biomaterials. 2006;27:2776–86.
5. Khang G, Kim MS, Bang H. A manual for biomaterials/scaffold fabrication technology. 1st ed. New Jersey: World scientific publishing company; 2007.
6. Sill TJ, Recum HA. Electrospinning: applications in drug delivery and tissue engineering. Biomaterials. 2008;29:1989–2006.
7. Heikkil P, Harlin A. Macromolecular nanotechnology: parameter study of electrospinning of polyamide-6. Eur Polym J. 2008;44:3067–79.
8. Sell S, Barnes C, Simpson D, Bowlin G. Scaffold permeability as a means to determine fiber diameter and pore size of electrospun fibrinogen. J Biomed Mater Res Part A. 2007;85:115–26.
9. Lannutti J, Reneker D, Ma T, Tomasko D, Farson D. Electrospinning for tissue engineering scaffolds. Mater Sci Eng C. 2007;27:504–9.
10. Lemon G, Waters SL, Rose FR, King JR. Mathematical modelling of human mesenchymal stem cell proliferation and differentiation inside artificial porous scaffolds. J Theor Biol. 2007;249:543–53.
11. Safinia L, Mantalaris A, Bismarck A. Nondestructive technique for the characterization of the pore size distribution of soft porous constructs for tissue engineering. Langmuir. 2006;22:3235–42.
12. Moore MJ, Jabbari E, Ritman EL, Lu L, Currier BL, Windebank AJ, et al. Quantitative analysis of interconnectivity of porous biodegradable scaffolds with micro-computed tomography. J Biomed Mater Res Part A. 2004;71:258–67.
13. Ziabari M, Mottaghitalab V, Haghi AK. Evaluation of electrospun nanofiber pore structure parameters. Korean J Chem Eng. 2008;25:923–32.
14. Tian F, Hosseinkhani H, Estrada G, Kobayashi H. Quantitative method for the analysis of cell attachment using aligned scaffold structures. J Phys Conf Ser. 2007;61:587–90.
15. Theron SA, Zussman E, Yarin AL. Experimental investigation of the governing parameters in the electrospinning of polymer solutions. Polymer. 2004;45:2017–30.
16. Ojha SS, Afshari M, Kotek R, Gorga RE. Morphology of electrospun nylon-6 nanofibers as a function of molecular weight and processing parameters. J Appl Polym Sci. 2008;108:308–19.
17. Gu SY, Ren J, Vancso GJ. Process optimization and empirical modeling for electrospun polyacrylonitrile (PAN) nanofiber precursor of carbon nanofibers. Eur Polym J. 2005;41:2559–68.
18. Tan S, Inai R, Kotaki M, Ramakrishna S. Systematic parameter study for ultrafine fiber fabrication via electrospinning process. Polymer. 2005;46:6128–34.
19. Deitzel JM, Kleinmeyer J, Harris D, Tan NB. The effect of processing variables on the morphology of electrospun nanofibers and textiles. Polymer. 2001;42:261–72.
20. Tehrani AH, Zadhoush A, Karbasi S, Khorasani SN. Experimental investigation of governing parameters in electrospinning poly(3-hydroxybutyrate) scaffolds: structural characteristics of the pores. J Appl Polym Sci 2010; doi:10.1002/app32620.
21. Dierickx W. Opening size determination of technical textiles used in agricultural applications. Geotext Geomembr. 1999;17:231–45.
22. Ziabari M, Mottaghitalab V, Haghi AK. Simulated image of electrospun nonwoven web of PVA and corresponding nanofiber diameter distribution. Korean J Chem Eng. 2008;25:919–22.
23. Mobarakeh LG, Semnani D, Morshed M. A novel method for porosity measurement of various surface layers of nanofibers mat using image analysis for tissue engineering applications. J Appl Polym Sci. 2007;106:2536–42.
24. Sengers BG, Taylor M, Please CP, Oreffo ROC. Computational modelling of cell spreading and tissue regeneration in porous scaffolds. Biomaterials. 2007;28:1926–40.
25. Sun W, Lal P. Recent development on computer aided tissue engineering—a review. Comput Methods Programs Biomed. 2002;67:85–103.
26. Sengers BG, Oomens OWJ, Baaijens FPT. An integrated finite element approach to mechanics, transport and biosynthesis in tissue engineering. J Biomech Eng. 2004;126:82–91.
27. Wilson CG, Bonassar LJ, Kohles SS. Modeling the dynamic composition of engineered cartilage. Arch Biochem Biophys. 2002;408:246–54.

28. Ajaal TT, Smith RW. Employing the Taguchi method in optimizing the scaffold production process for artificial bone grafts. J Mater Process Technol. 2009;209:1521–32.
29. Hsieh KL, Tong LI, Chiu HP, Yeh HY. Optimization of a multiresponse problem in Taguchi's dynamic system. Comput Ind Eng. 2005;49:556–71.
30. Ritter HL, Drake C. Pore-size distribution in porous materials. Ind Eng Chem. 1945;17:782–6.
31. Li WJ, Laurencin CT, Caterson EJ, Tuan RS, Ko FK. Electrospun nanofibrous structure: a novel scaffold for tissue engineering. Biomed Mater Res. 2002;60:613–21.
32. Jones JR, Poologasundarampillai G, Atwood RC, Bernard D, Lee PD. Non-destructive quantitative 3D analysis for the optimization of tissue scaffolds. Biomaterials. 2007;28:1404–13.
33. Xi SJ. A control approach for pore size distribution in the bone scaffold based on the hexahedral mesh refinement. Comput Aided Des. 2008;40:1040–50.
34. Blacher S, Maquet V, Schils F, Martin D, Schoenen J, Moonen G, et al. Image analysis of the axonal ingrowth into poly(d, l-lactide) porous scaffolds in relation to the 3-D porous structure. Biomaterials. 2003;24:1033–40.
35. Karageorgiou V, Kaplan D. Porosity of 3D biomaterial scaffolds and osteogenesis. Biomaterials. 2005;26:5474–91.
36. Badami AS, Kreke MR, Thompson MS, Riffle JS, Goldstein AS. Effect of fiber diameter on spreading, proliferation, and differentiation of osteoblastic cells on electrospun poly(lactic acid) substrates. Biomaterials. 2006;27:596–606.
37. Wan Y, Wang Y, Liu Z, Qu X, Han B, Bei J, et al. Adhesion and proliferation of OCT-1 osteoblast-like cells on micro- and nanoscale topography structured poly(L-lactide). Biomaterials. 2005;26:4453–9.
38. O'Brien FJ, Harley BA, Yannas IV, Gibson LJ. The effect of pore size on cell adhesion in collagen-GAG scaffolds. Biomaterials. 2005;26:433–41.
39. Suwantong O, Waleetorncheepsawat S, Sanchavanakit N, Pavasant P, Cheepsunthorn P, Bunaprasert T, et al. In vitro biocompatibility of electrospun poly(3-hydroxybutyrate) and poly(3-hydroxybutyrate-*co*-3-hydroxyvalerate) fiber mats. Int J Biol Macromol. 2007;40:217–23.
40. Sombatmankhong K, Sanchavanakit N, Pavasant P, Supaphol P. Bone scaffolds from electrospun fiber mats of poly(3-hydroxybutyrate), poly(3-hydroxybutyrate-co-3-hydroxyvalerate) and their blend. Polymer. 2007;48:1419–27.
41. Sajeev US, Anand KA, Menon D, Nair S. Control of nanostructures in PVA PVA/chitosan blends and PCl through electrospinning. Bull Mater Sci. 2008;31:343–51.
42. Venugopal J, Ramakrishna S. Applications of polymer nanofibers in biomedicine and biotechnology. Appl Biochem Biotechnol. 2005;125:147–57.